Draft Version February 16, 2018
Preprint typeset using LaTeX style emulateapj v. 12/16/11

PLANCK CLUSTER PAPER

SB[1], JPH[1], FM, PD[1]

Draft Version February 16, 2018

ABSTRACT

We propose to continue our program of optical imaging to unveil all of the most massive clusters in the observable Universe. We start from the all-sky Planck Sunyaev-Zeldovich (SZ) catalogs, which contain several hundred high significance (signal-to-noise ratio, SNR > 5) unconfirmed cluster candidates. Since SZ selection favors high mass clusters and the Planck confirmation process favored low redshift systems, the highest significance unconfirmed candidates are, therefore, likely massive clusters ($M_{500} > 5 \times 10^{14}$ M$_\odot$) at relatively high redshift ($z > 0.5$). Our proposed observations, using MOSAIC-3 on Mayall, are designed to confirm the presence of a brightest cluster galaxy (to $z \sim 1$) and red sequence of accompanying cluster members (to $z \sim 0.7$). Preliminary results from our observations over the past two years have validated our approach by the detection of optical clusters in a number of Planck candidates, including the discovery of rich systems at $z = 0.553$ and $z = 0.830$ that rival the most massive clusters known. The proposed observations represent the first step required to provide a complete all-sky census throughout the observable Universe of the most massive, high redshift clusters. Their expected high redshift and high mass make the unconfirmed Planck clusters, arguably, the most important available sample for probing deviations from ΛCDM and defining the high-mass end of the cluster mass function.
Subject headings:

1. INTRODUCTION

this section has not been edited and is just a bunch of stuff copy and pasted. I did update some of the references. Massive galaxy clusters at high redshifts are rare beasts that hold important clues to the evolution of structure in the Universe and in principle can help probe (or falsify) structure formation models under the ΛCDM paradigm (e.g., Mortonson et al. 2011; Harrison & Coles 2012; Harrison & Hotchkiss 2012; Waizmann et al. 2012; Zitrin et al. 2009). Galaxy clusters also harbor a significant fraction of the visible baryons in the Universe, in the form of a hot intracluster medium that leaves an imprint on the Cosmic Microwave Background (CMB) though the Sunyaev-Zel'dovich (SZ; Sunyaev & Zeldovich 1972 effect.

The surface brightness of the SZ effect does not depend on redshift, therefore providing uniform samples of massive clusters up to arbitrary distances. This has been borne out by the large area surveys of the Atacama Cosmology Telescope (ACT; Swetz et al. 2011) and the South Pole Telescope (SPT; Carlstrom et al. 2011 that have detected hundreds of massive clusters since 2008 up to redshifts of $z \sim 1.4$ (see Reichardt et al. 2013 and Hasselfield et al. 2013 for latest results). Now, Planck has released an all-sky SZ sample (PSZ; Planck Collaboration et al. 2014) that contains 861 confirmed clusters (of which most [683] were known previously) and another 366 unconfirmed cluster candidates.

We led the ACT cluster confirmation process using 4-m class telescopes; now we propose to use our well-established expertise to identify Planck clusters. The recent SZ cluster samples have opened a new window into extreme systems, the most massive clusters at high redshift (Foley et al. 2011; Menanteau et al. 2012), prompting studies that match their observed numbers with the abundance predictions of ΛCDM cosmology (Hoyle et al. 2011, Mortonson et al. 2011, Waizmann et al. 2012). There are few, if any, clusters at high redshift ($z > 0.8$) and high mass ($M_{200} > 10^{15}$ M$_\odot$) in the cosmological simulations (see Tinker et al. 2008), so the halo mass function at high-z and high-M is essentially unconstrained. Thus, with the proposed observations we will determine the abundance of massive clusters at high redshift making a direct observational measurement of the high-z, high-M end of the halo mass function. For example, one of the most impressive results of the ACT SZ survey is our discovery of the high redshift ($z = 0.87$), extreme cluster "El Gordo" (ACT-CL J0102-4915), the most significant SZ detection of the whole survey (and also of the SPT survey). Our recent HST weak-lensing analysis has provided an independent mass estimation $M_{200a} = (3.1 \pm 0.7) \times 10^{15}$ M$_\odot$ (Jee et al. 2013) that confirms our earlier mass estimates for the cluster (Menanteau et al. 2012). Based on its estimated mass alone, "El Gordo" is a very rare system within the ACT+SPT (2800 sq. deg.) survey area, but is still consistent with the expectations of ΛCDM. We are now at a unique moment in cluster science where we can discover all massive clusters in the observable universe. This census will measure the high-mass, high-redshift cluster mass function, and determine the extent of deviations from the theoretical halo mass function (Jenkins et al. 2001; Tinker et al. 2008).

Assuming WMAP7 cosmology (Komatsu et al. 2011) with the Tinker et al. (2008) halo mass function, there should be only ~ 4 clusters as massive as El Gordo ($\leq 2 \times 10^{15}$ M$_\odot$) at $z > 0.6$ in the full area covered by the Planck PSZ catalog (83.7% of the sky). Although Plancks larger beam size (compared to both ACT and SPT) makes it more sensitive to clusters at lower red-

[1] Rutgers;boada@physics.tamu.edu

shifts (due to their larger projected area on the sky), among the 861 confirmed clusters in the recently released all-sky Planck SZ catalog are the two highest significance high-redshift SZ detections from ACT (as well as several other ACT and SPT clusters). This confirms the ability of Planck to unambiguously detect the most massive clusters at high redshift. In fact Planck reports "El Gordo" ($z = 0.87$) and ACT-CL J2327.40204 ($z = 0.701$) at S/N values of 8.0 and 6.3, respectively. And as Figure 2 (right panel) shows, these are the two most massive Planck clusters in the confirmed sample at high redshift. For the new clusters we confirm, our experimental design allows us to estimate photometric redshifts, which will be sufficiently accurate for a meaningful estimate of the clusters mass from the Planck SZ signal.

Unless otherwise noted, throughout this paper, we use a concordance cosmological model ($\Omega_\Lambda = 0.7$, $\Omega_m = 0.3$, and $H_0 = 70$ km s^{-1}Mpc^{-1}), assume a Chabrier initial mass function (Chabrier 2003), and use AB magnitudes (Oke 1974).

2. DESIGN

Among the recently released, second, all-sky PSZ catalog (Planck Collaboration et al. 2016) there are 366 unconfirmed SZ detections with S/N > 4.5. The vast majority of these must lie at high-z because the Planck confirmation process mostly relied on existing catalogs with a preference for low-z clusters. Furthermore, the confirmed sample has a small fraction (3%) of $z > 0.6$ clusters compared to that expected ($\sim 20\%$) based on the theoretical halo mass function (Jenkins et al. 2001; Tinker et al. 2008). If other clusters like "El Gordo" exist, they are hiding as high-significance candidates within the objects in this catalog. The design of the observations is to use both optical and near-infrared (NIR) imaging to confirm the SZ detections as real clusters and provide photometric redshifts using the multi-color information.

Our strategy is to use the Kitt Peak National Observatory (KPNO) Mayall-4m telescope imaging as the first and fundamental step to confirm the highest significance detections in the PSZ catalog that are visible across the entire northern sky. Following closely the procedure used for ACT follow-up citation?, targets are prioritized by SZ signal-to-noise (S/N). We choose to initially report on targets with PSZ S/N> 5 as the statistical reliability of PSZ cluster candidates is quite high: according to the Planck team $\sim 90\%$ of candidates at S/N> 5 turn out to be "real" clusters (citation? maybe show the figure from the proposal).

Optical imaging will be sufficient to confirm nearly all of the candidates, but for the highest redshift ones, NIR data will be necessary. Again following the procedure for ACT cluster follow-up: those candidates with some evidence for a high-z brightest cluster galaxy (BCG; note that we can detect BCGs to $z \sim 1.5$) will be targeted with NIR observations to confirm the presence of a BCG and detect the red sequence of cluster members. Observational priority again is given to higher S/N candidates.

2.1. *Observations*

All observations were conducted with the KPNO Mayall telescope. The optical observations were made with the MOSAIC camera mounted at the prime focus. Two detector packages were used for the observations. The earlier MOSAIC1.1 instrument consisted of eight 2048×4096 SITe CCDs, arranged 2×4, separated by a ~ 50 pixels gap with a pixel scale of $0\farcs26$ pixel^{-1}. MOSAIC1.1 was replaced with Mosaic3, in year?, and consists of four new 4k×4k, 15 micron pixel, 500-micron thick LBNL deep-depletion CCDs. Because the only change from MOSAIC1.1 to MOSAIC3 are the CCDs and controllers the both versions have a $36' \times 36'$ field-of-view.

The near-IR observations utilized the National Optical Astronomy Observatory (NOAO) Extremely Wide-Field Infrared Imager (NEWFIRM; Probst et al. 2004). The instrument consists of four InSb 2048×2048 pixel arrays arranged in 2×2 with approximately $1'$ gaps between each of the CCDs. The detector has a plate scale of $0\farcs4$ pixel^{-1} and a $28' \times 28'$ field-of-view.

need to talk about the dithering

The optical observing strategy consists of targeted *griz* observations of individual candidates with exposure times of 350 s, 350 s, 1100 s and 1100 s (assuming dark conditions) to provide 5σ detections limits of g =??, $r = 24.5$, $i = 24.5$, $z = 24.2$ ensuring the unambiguous detection of the faint (i.e., 0.4L$\star$) galaxies in the red cluster sequence up to $z \sim 1.0$ (citation?) and of brightest cluster galaxies (BCGs) to higher redshifts. The choice of filters in our program is driven by the need to segregate early-type galaxies in the cluster through their colors (or photometric redshifts) by sampling blueward and red-ward of the 4000Å break.

For the NEWFIRM observations, we obtained 3600 s of Ks band imaging using 60 s exposures (5 coadded 12 s exposures) taken at 60 different dither positions distributed quasi-randomly over a square $100'' \times 100''$ region. This produced reduced images with uniform exposure and sky level. The final dithered images cover approximately $28' \times 28'$ which comfortably matches the MOSAIC observations.

A NEWFIRM integration of 3600 s allows us to reach a limiting Ks magnitude of ~ 22.0 (AB, 3σ). This magnitude limit corresponds to $\sim M_\star + 2$ in the cluster luminosity function at $z = 1.0$ as measured by De Propris et al. (1999), and assuming Ks AB = Ks Vega +1.86. This surface brightness limit corresponds to $\sim M_\star + 1.0$ at $z = 1.5$, sufficient for detecting sub L$_\star$ at this limit, allowing for confident detection of the BCG and associated red cluster sequence.

TABLE 1 Basic properties of the galaxy clusters candidates targeted for observation with the MOSAIC and NEWFIRM instruments: Column 1: Cluster name; Column 2: The right ascension of the cluster; Column 3: The declination of the cluster; Column 4: the PSZ catalog S/N ratio; Column 5: The date of MOSAIC observations; Column 6: The data of NEWFIRM observations.

Cluster (1)	RA (J2000) (2)	DEC (J2000) (3)	PSZ1 SNR (4)	PSZ2 SNR (5)	MOSAIC Obs. (6)	NEWFIRM Obs. (7)
PSZ1_G031.91+67.94	14:29:02	+24:37:33.38	5.23	...	Feb, 2014	Feb, 2016

TABLE 1 Continued

Cluster (1)	RA (J2000) (2)	DEC (J2000) (3)	PSZ1 SNR (4)	PSZ2 SNR (5)	MOSAIC Obs. (6)	NEWFIRM Obs. (7)
PSZ1_G055.83-41.64	21:57:14	-2:31:51	5.72	...	Oct, 2014	Nov, 2014
PSZ1_G084.62-15.86	21:49:44	+33:10:23.81	6.01	...	Oct, 2014	...
PSZ1_G096.44-10.40	22:19:35	+44:31:05.27	6.55	...	Oct, 2014	Nov, 2014
PSZ1_G102.86-31.07	23:33:08	+28:43:51.60	6.12	...	Oct, 2014	Nov, 2014
PSZ1_G102.97-04.77	22:34:47	+52:43:13.90	5.64	...	Oct, 2014	...
PSZ1_G105.91-38.39	23:53:54	+22:34:21.09	7.16	...	Oct, 2014	Nov, 2014
PSZ1_G108.90-52.04	0:16:38	+09:52:49.98	6.89	...	Jun, 2017	Nov, 2014
PSZ1_G118.06+31.10	15:54:34	+84:10:37.49	6.00	...	Feb, 2014	Mar, 2014
PSZ1_G125.54-56.25	0:57:17	+06:35:23.29	4.86	...	Nov, 2014	...
PSZ1_G127.55+20.84	3:10:51	+82:25:43.91	5.91	...	Oct, 2014	Nov, 2014
PSZ1_G138.60-10.85	2:27:02	+49:04:54.07	8.26	...	Oct, 2014	Nov, 2014
PSZ1_G142.17+37.28	9:18:56	+70:52:01.14	5.79	...	Feb, 2014	Mar, 2014
PSZ1_G142.38+22.82	6:13:40	+71:52:21.02	5.82	...	Feb, 2014	Mar, 2014
PSZ1_G146.00-49.42	1:51:35	+10:44:02.79	6.62	...	Oct, 2014	Nov, 2014
PSZ1_G148.20+23.49	6:37:46	+66:54:24.40	8.40	...	Feb, 2014	Mar, 2014
PSZ1_G153.41+36.58	8:42:40	+62:34:31.61	6.85	...	Feb, 2014	Mar, 2014
PSZ1_G153.56+36.32	8:39:31	+62:31:30.58	5.96	...	Feb, 2014	Mar, 2014
PSZ1_G162.30-26.92	3:24:26	+24:00:44.46	6.56	...	Oct, 2014	Nov, 2014
PSZ1_G169.80+26.10	7:30:08	+48:20:02.06	5.32	...	Oct, 2014	...
PSZ1_G182.49-57.09	2:44:20	-7:55:37	5.09	...	Nov, 2014	...
PSZ1_G183.26+12.25	6:42:56	+31:49:07.58	5.43	...	Oct, 2014	...
PSZ1_G185.93-31.21	4:11:39	+06:16:00.67	5.90	...	Jan, 2014	Nov, 2014
PSZ1_G206.45+13.89	7:29:59	+11:56:22.64	5.90	...	Feb, 2014	Mar, 2014
PSZ1_G206.64-21.17	5:24:49	-4:14:07	6.62	...	...	Dec, 2014
PSZ1_G224.82+13.62	8:01:42	-4:03:54	5.51	...	Jan, 2014	...
PSZ1_G244.48+34.06	9:49:52	-7:29:28	8.14	...	Jan, 2014	Mar, 2014
PSZ1_G249.01+73.75	11:56:46	+16:55:43.68	7.14	...	Feb, 2014	Mar, 2014
PSZ1_G286.25+62.68	12:21:10	+00:47:34.05	5.52	...	Feb, 2014	Feb, 2016
PSZ1_G341.69+50.66	14:25:20	-4:59:54	5.48	...	Feb, 2014	...
PSZ2_G022.03+17.75	17:28:37	-1:13:03	5.64	6.20	Jun, 2017	Feb, 2016
PSZ2_G023.05+20.52	17:20:47	+00:58:06.58	...	5.57	Jun, 2017	...
PSZ2_G024.46-18.08	19:42:23	-15:26:09	...	6.98	Jun, 2017	...
PSZ2_G027.77+10.88	18:03:22	+00:25:57.59	...	6.42	Jun, 2016	...
PSZ2_G028.15-08.62	19:13:41	-8:08:26	5.07	7.67	Jun, 2017	...
PSZ2_G029.66-47.63	21:45:44	-21:46:49	...	5.74	Nov, 2016	...
PSZ2_G029.80-17.40	19:48:32	-10:31:40	6.59	9.01	Jun, 2016	...
PSZ2_G031.41-19.16	19:57:41	-9:53:56	4.60	5.69	Jun, 2017	...
PSZ2_G032.12-14.96	19:43:34	-7:27:45	8.21	9.12	Jun, 2017	Nov, 2016
PSZ2_G032.31+66.07	14:37:11	+24:23:21.25	...	5.14	...	Jan, 2017
PSZ2_G033.27-17.54	19:54:52	-7:36:11	5.78	6.86	Jun, 2017	...
PSZ2_G036.69-15.67	19:54:05	-3:50:23	...	5.69	Jun, 2017	...
PSZ2_G043.44-41.27	21:36:44	-10:17:48	...	5.55	Jun, 2017	...
PSZ2_G044.83+10.02	18:36:39	+15:04:49.72	7.27	9.27	Oct, 2015	Feb, 2016
PSZ2_G045.50-08.62	19:45:25	+07:04:29.08	4.57	5.63	Jun, 2017	...
PSZ2_G047.53+08.55	18:46:59	+16:50:35.39	5.82	6.55	Jun, 2016	...
PSZ2_G048.47+34.86	17:02:08	+27:08:48.05	...	5.74	Jun, 2016	Feb, 2016
PSZ2_G065.35-08.01	20:26:04	+24:08:06.72	...	5.83	Jun, 2016	...
PSZ2_G071.67-42.76	22:30:54	+05:42:05.22	8.82	8.63	Oct, 2014	Nov, 2014
PSZ2_G075.08+19.83	18:46:48	+45:46:33.27	...	5.74	Jun, 2016	...
PSZ2_G086.35-13.94	21:49:44	+35:42:37.49	...	5.42	...	Nov, 2016
PSZ2_G089.06-11.79	21:52:53	+39:03:52.50	...	5.72	Nov, 2016	...
PSZ2_G092.11-33.73	23:01:37	+22:28:59.71	...	5.81	Nov, 2016	Nov, 2016
PSZ2_G092.46-35.22	23:05:50	+21:19:27.96	5.47	6.73	Oct, 2014	Nov, 2014
PSZ2_G093.04-32.38	23:01:43	+24:02:24.90	5.69	6.03	Oct, 2014	Nov, 2014
PSZ2_G093.41-16.26	22:23:55	+38:00:25.32	...	4.59	...	Nov, 2016
PSZ2_G093.71-30.90	23:00:44	+25:36:40.92	...	5.00	...	Nov, 2016
PSZ2_G096.43-20.89	22:48:09	+35:33:21.47	...	5.81	Jun, 2016	Nov, 2016
PSZ2_G098.38+77.22	13:18:25	+38:35:06.94	4.71	5.51	Jun, 2017	Nov, 2016
PSZ2_G100.22+33.81	17:13:41	+69:22:24.33	...	5.69	Jun, 2017	...
PSZ2_G100.45+16.79	20:18:34	+66:47:07.85	...	11.79	Oct, 2015	Nov, 2015
PSZ2_G104.15-38.85	23:48:48	+21:43:24.60	...	6.41	Jun, 2016	Nov, 2016
PSZ2_G106.11+24.11	19:21:24	+74:33:21.87	...	5.70	Jun, 2017	...
PSZ2_G107.41-09.57	23:13:47	+50:19:32.01	...	10.69	Jun, 2016	Nov, 2015
PSZ2_G107.83-45.45	0:07:35	+16:07:51.05	...	7.09	Nov, 2016	Nov, 2016
PSZ2_G112.07-39.86	0:15:30	+22:14:43.50	...	5.72	Nov, 2016	Nov, 2016
PSZ2_G112.54+59.53	13:29:54	+56:48:44.45	...	5.37	...	Jan, 2017
PSZ2_G120.76+44.14	13:12:39	+72:53:23.47	...	5.59	Jun, 2017	Feb, 2016
PSZ2_G123.35+25.39	1:41:20	+88:13:14.57	5.90	10.86	Oct, 2014	Feb, 2016
PSZ2_G123.84+25.75	2:55:30	+88:24:01.91	5.04	5.81	Nov, 2016	Feb, 2016
PSZ2_G124.11+25.02	2:40:03	+87:38:38.73	...	5.53	...	Nov, 2016
PSZ2_G125.55+32.72	11:25:35	+83:57:29.12	...	6.49	Nov, 2016	Feb, 2016
PSZ2_G127.35-10.69	1:19:42	+51:56:15.39	5.58	6.94	Oct, 2014	Nov, 2014
PSZ2_G128.15-24.71	1:15:30	+37:54:48.45	...	4.75	...	Nov, 2016
PSZ2_G131.27-25.82	1:28:49	+36:26:41.01	...	4.50	...	Nov, 2016
PSZ2_G135.94-68.22	1:10:42	-5:50:45	...	6.87	...	Jan, 2017
PSZ2_G136.31+54.67	11:47:50	+60:45:56.07	...	6.92	Jun, 2017	Feb, 2016
PSZ2_G137.24+53.93	11:41:07	+61:11:39.02	...	7.87	Nov, 2016	Feb, 2016

TABLE 1 Continued

Cluster (1)	RA (J2000) (2)	DEC (J2000) (3)	PSZ1 SNR (4)	PSZ2 SNR (5)	MOSAIC Obs. (6)	NEWFIRM Obs. (7)
PSZ2_G137.58+53.88	11:39:27	+61:09:01.04	5.73	8.18	Feb, 2014	Mar, 2014
PSZ2_G139.72-17.13	2:19:55	+42:49:53.97	...	5.12	...	Nov, 2016
PSZ2_G144.84-35.16	2:09:42	+24:21:19.56	...	4.84	...	Nov, 2016
PSZ2_G145.25+50.84	10:53:26	+60:51:43.24	...	5.98	Jun, 2017	Feb, 2016
PSZ2_G146.88+17.13	5:34:10	+65:43:14.28	...	6.13	Nov, 2016	Feb, 2016
PSZ2_G153.56+36.82	8:44:32	+62:24:41.96	...	15.90	Nov, 2016	Nov, 2015
PSZ2_G153.68+36.96	8:45:33	+62:17:12.13	...	5.07	Nov, 2016	Nov, 2015
PSZ2_G163.22-26.48	3:28:29	+23:50:15.15	...	6.35	Nov, 2016	Feb, 2016
PSZ2_G165.39+09.22	5:47:59	+46:08:39.24	...	5.60	Nov, 2016	Nov, 2016
PSZ2_G166.27-24.71	3:42:39	+23:24:41.39	...	9.58	Nov, 2016	Nov, 2015
PSZ2_G166.27-25.02	3:41:44	+23:11:00.45	...	8.09	Nov, 2016	Nov, 2016
PSZ2_G166.56-17.69	4:04:47	+28:21:38.16	...	4.76	...	Nov, 2016
PSZ2_G167.44-38.06	3:09:12	+12:37:11.49	6.11	7.66	Oct, 2014	...
PSZ2_G171.79-42.08	3:08:40	+07:24:32.96	...	5.84	Nov, 2016	Feb, 2016
PSZ2_G173.76+22.92	7:17:28	+44:03:27.62	...	5.80	Nov, 2016	Feb, 2016
PSZ2_G179.33-22.22	4:25:30	+16:27:52.77	...	5.02	...	Jan, 2017
PSZ2_G181.88-30.77	4:04:21	+09:16:14.87	...	9.29	Nov, 2016	Nov, 2015
PSZ2_G183.92+16.36	7:01:57	+32:51:35.39	...	4.97	...	Nov, 2016
PSZ2_G185.45-32.01	4:08:04	+06:06:33.99	6.15	4.99	Jan, 2014	Nov, 2014
PSZ2_G189.79-37.25	3:59:37	+00:07:54.80	6.99	7.28	Oct, 2014	Nov, 2014
PSZ2_G191.57+58.88	10:29:40	+33:54:35.76	...	5.17	...	Jan, 2017
PSZ2_G191.82-26.64	4:38:37	+04:42:02.64	4.76	6.17	Nov, 2016	Feb, 2016
PSZ2_G192.40-67.89	2:18:20	-17:45:23	...	7.03	Nov, 2016	Feb, 2017
PSZ2_G194.68-49.76	3:25:22	-9:40:50	5.00	5.71	Nov, 2016	Nov, 2016
PSZ2_G203.32+08.91	7:06:10	+12:33:14.21	...	5.15	...	Jan, 2017
PSZ2_G210.37-37.00	4:32:44	-14:03:01	...	9.84	Nov, 2016	Nov, 2015
PSZ2_G210.71+63.08	10:51:42	+24:58:09.19	...	7.37	Jun, 2017	Feb, 2016
PSZ2_G210.78-36.25	4:36:07	-14:02:58	...	6.32	Nov, 2016	Feb, 2016
PSZ2_G216.25+10.10	7:33:26	+01:40:36.28	5.16	5.52	...	Nov, 2016
PSZ2_G228.35-66.31	2:38:41	-30:50:21	...	9.08	...	Nov, 2016
PSZ2_G230.28-28.57	5:31:09	-26:49:29	...	9.30	...	Nov, 2016
PSZ2_G235.96+38.21	9:46:11	+00:29:10.03	4.79	9.40	...	Feb, 2016
PSZ2_G237.68+57.83	10:53:31	+10:48:56.98	...	5.36	...	Jan, 2017
PSZ2_G246.86-12.29	7:08:10	-35:37:39	7.46	7.86	...	Dec, 2014
PSZ2_G252.45+73.44	11:58:35	+16:00:18.38	...	5.57	Jun, 2017	Feb, 2016
PSZ2_G253.44-10.93	7:28:33	-40:51:17	6.26	7.08	...	Dec, 2014
PSZ2_G254.52+62.52	11:29:57	+07:35:04.97	...	4.85	...	Jan, 2017
PSZ2_G270.88+37.23	11:05:19	-18:56:55	...	5.49	...	Jan, 2017
PSZ2_G305.76+44.79	12:59:54	-18:01:59	4.72	5.72	Jun, 2017	Feb, 2016
PSZ2_G310.81+83.91	12:55:01	+21:05:41.16	...	8.29	Nov, 2016	Feb, 2016
PSZ2_G318.46+83.79	12:58:33	+21:08:11.93	6.93	9.40	Feb, 2014	Mar, 2014
PSZ2_G320.94+83.69	12:59:47	+21:06:56.63	...	7.32	Jun, 2017	Feb, 2016
PSZ2_G328.96+71.97	13:23:13	+10:43:41.59	...	5.85	Jun, 2017	Feb, 2016

A summary of our observations is given in Table 1.

3. DATA REDUCTION AND CALIBRATION

Standard image reductions including subtraction of dark frames, flat fielding, sky-subtraction, and bad pixel masking was performed by the NOAO virtual observatory using the MOSAIC (Valdes & Swaters 2007) and NEWFIRM (Swaters et al. 2009) science pipelines. The resultant FITS files consist of fully reduced images with either all single exposure CCDs mosaicked into a single image extension (as in the case of Mosaic1.1 and NEWFIRM) or as a multi-extension FITS file with each single exposure CCD occupying a separate extension.

We then mosaic each separate exposure into a master mosaic as described in the following section.

3.1. *Mosaicking*

Combined mosaics are created with SWARP (Bertin et al. 2002). We create three distinct types of mosaics. The individual dither frames are stacked and then median combined to produce the final completed science mosaic. A "detection" is created by combining select science mosaics into a chi2 image using either the i-band and Ks-band or $i-$ and z-band when Ks imaging is not available. Finally we create a set of mosaics use to produce the three color image used for cluster detection. For this we median combine the $griz$ and Ks science mosaics into a "blue" (gr-bands), "green" ($iz-bands$), and "red" (Ks-band) mosaic. All final mosaics have a pixelscale of $0\farcs25$/pix. The final exposure time is calculated as the median exposure time of the combined images, and similarly the final airmass is median of the individual air masses. need to talk about the weight images

The full parameter file used while creating the mosaics is given in Appendix **??**.

3.2. *Astrometric Calibration*

Each of the final science mosaics produced in the previous section are first astrometrically aligned with *Gaia* (Gaia Collaboration et al. 2016a) Data Release 1 (Gaia Collaboration et al. 2016b) using SCAMP (Bertin 2006) as a part of PHOTOMETRYPIPELINE (PP; Mommert & M. 2017). footnote to github

Sources are extracted from the mosaics with a signal-to-noise ratio (SNR) of at least ten and with a minimum area of at least 12 pixels. The extracted sources are then matched to the *Gaia* data and a new astrometric solution is calculated. Because the initial astrometric solution from the VO is quite accurate, the resultant corrections are much less than $1''$.

3.3. *Photometric Calibration*

After the mosaics have been astrometrically aligned, we use PP to produce a photometric solution. PP calculates a photometric zero-point in each of our observed bands by comparing field stars located throughout the mosaic to known photometry from large-area sky surveys. Because our sources are spread across the entire northern sky, and because we prefer to minimize the number of differences between photometric solutions we are limited to two optical surveys and a single IR survey. For the optical data, we first seek photometric data from the *Sloan Digital Sky Survey* (SDSS; York et al. 2000) Data Release 13 (Alam et al. 2015) get a new citation for dr13 this is for dr12. When our target does not lie within the SDSS footprint we utilize the Panoramic Survey Telescope and Rapid Response System (Pan-STARRS; Chambers et al. 2016) Data Release 1 (hereafter PS1; Flewelling et al. 2016). Both surveys provide accurate *griz* magnitudes and large on-line queriable databases for rapid automated calibration. For our IR imaging, we rely on the *Two Micron All Sky Survey* (2MASS; Skrutskie et al. 2006).

Sources are extracted from the combined mosaics with either a $3''$ or $8''$ diameter aperture for optical and IR sources respectively; sources with a SNR$\geq$ 10 are matched to a survey catalog and a photometric zero-point is determined. We use half of the available stars (with accurate catalog photometry) to derive the zero-point resulting in zero-points calculated from approximately $10-500$ stars and with typical uncertainties of give zp errors in the different bands.

Should we talk about the difference between us and SDSS? If so, how should we "sum up" the differences in a simple way?

4. ANALYSIS

Lorem ipsum dolor amet swag copper mug meh tilde, put a bird on it live-edge tattooed kinfolk before they sold out locavore selvage leggings raclette literally bicycle rights. Hot chicken kickstarter mustache vinyl roof party. Wayfarers brooklyn truffaut twee umami, venmo irony. Typewriter viral pop-up, listicle vaporware organic af salvia keytar twee chillwave austin +1 offal blog. La croix dreamcatcher snackwave, try-hard intelligentsia taxidermy messenger bag air plant godard mustache celiac glossier echo park. Photo booth readymade authentic glossier biodiesel snackwave beard hammock sriracha before they sold out edison bulb fixie PBR&B. Man bun pabst kogi, crucifix subway tile af tacos cray tumeric lyft cronut lomo tattooed.

4.1. *Source Extraction and Photometry*

For source extraction and photometry estimation we use Source Extractor (hereafter SExtractor; version 2.19.5; Bertin & Arnouts 1996) run dual image mode with the CHI2 detection image as the detection image. See Section 3.1. See Appendix **??** for a complete parameter listing.

4.2. *Photometric Redshifts*

We determine photometric redshifts (photo-z) from the five-band optical and IR (when available) images using Bayesian Photometric Redshifts (BPZ; Benitez 2000; Coe et al. 2006) following the same procedure as in Menanteau et al. (2009).

We assess the effectiveness of our photo-z estimates by comparing with the available spectroscopic redshifts (spec-z) from the SDSS. We use three diagnostics to gauge photo-z accuracy. First, we report the full scatter between the photo-z and spec-z, defined as:

$$\sigma_f = \mathrm{RMS}[\delta z/(1+z_{spec})] \quad (1)$$

where $\delta z = z_{spec} - z_{phot}$. Second, we report the normalized median absolute deviation (NMAD; Ilbert et al. 2009; Dahlen et al. 2013; Molino et al. 2017), given as

$$\sigma_{NMAD} = 1.48 \times \mathrm{median}\left(\frac{|\delta z|}{1+z_{spec}}\right). \quad (2)$$

which provides an estimate of the scatter resistant to catastrophic outliers. Finally, the catastrophic outlier fraction (OLF) where we define a catastrophic outlier (following Molino et al. 2017) as,

$$\eta = \frac{|\delta z|}{(1+z_{spec})} > 5 \times \sigma_{NMAD}. \quad (3)$$

Figure 1 shows the photometric redshift performance as a function of the true spectroscopic redshift. For the full sample of galaxies we calculate $\sigma_f = XX\%$, $\sigma_{NMAD} = XX\%$, and an outlier fraction, $\eta = XX\%$. When considering the performance of only the galaxies BPZ classified as E and E/S0 type, we find the following results; $\sigma_f = 10.4\%$, $\sigma_{NMAD} = 5.43\%$, and an outlier fraction, $\eta = 2.97\%$.

4.3. *Cluster Finding*

In this section, we briefly describe the algorithms and methods use to select the galaxy clusters from the multi-wavelength optical/NIR imaging. We follow the methods described in detail in Menanteau et al. (2009, 2010a). We direct the reader there for an in depth description and discussion of the methods.

We first create a three-color image using STIFF (Bertin & Emmanuel 2011). The red, green, and blue channels are given by the corresponding combined mosaics described in Section 3.1. We then visually inspect an area of roughly $8' \times 8'$ centered on the position of each unconfirmed cluster; see Table 1. Potential brightest cluster galaxies (BCGs) are identified by first calculating the absolute limiting magnitude needs details.

Once a potential BCG is selected, the algorithm selects nearby galaxies, within $|z_{BCG} - z| < 0.05$ and 0.5 Mpc projected radius, which BPZ has classified as either E or E/S0 galaxies. These photo-z's of the galaxies are combined using a 3σ median sigma-clipping algorithm to estimate the cluster's mean redshift, z_c. We use this mean cluster redshift measurement and the member selection criteria given previously to estimate the number of cluster members within 1 Mpc, $N_{1\mathrm{Mpc}}$, which we define as the richness of the cluster, N_{gal}.

We correct the N_{gal} estimate by subtracting a statistical background of galaxies. We first estimate the number of background ellipticals by selecting galaxies within an annulus ($R_{200} < r < 2R_{200}$) around each cluster's position. We include galaxies with $\delta z = 0.05$ and similar colors as those galaxies assumed to belong to the cluster.

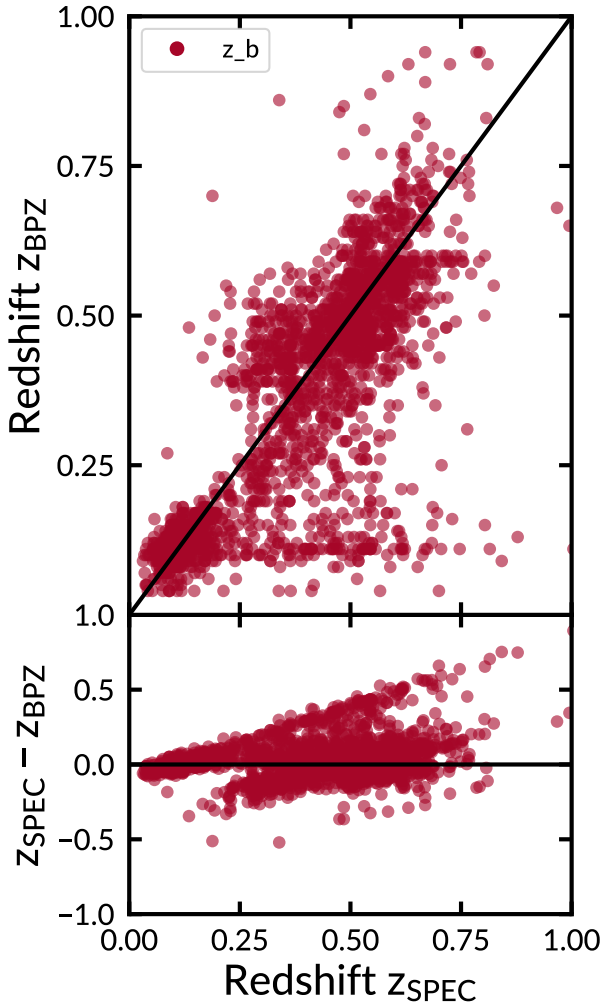

FIG. 1.— Comparison between photometric and spectroscopic redshifts for 2253 galaxies which have spectroscopic redshifts from the SDSS. The photometric redshifts in the top panel use a Bayesian approach with a custom empirical prior on galaxy brightness for the photometric redshifts. The bottom panel shows the difference between the spectroscopic and photometric redshift.

These galaxies are subtracted from the cluster's population which provides an corrected N_{gal}, N_{galc}, which we then use to compute other important quantities. In practice the corrected number of galaxies is between 15% and 20% lower than the uncorrected number (Menanteau et al. 2010a). We report N_{galc} for the remainder of this work.

4.4. *Recovery of the Brightest Cluster Galaxies*

We have designed our observations to detect BCGs to $z \sim 1.5$. To quantify the actual depth of our images, we perform a Monte Carlo simulation by injecting artificial elliptical galaxies and computing their recovery fraction. We create the artificial elliptical galaxies with the ARTDATA package, part of IRAF (Tody 1993).

Following the procedure given in Menanteau et al. (2010b), the synthetic galaxies are created with GALLIST to have de Vaucouleurs (de Vaucouleurs 1948) profiles and surface brightnesses corresponding to their magnitude and assumed sizes. The MKOBJECTS task injects artificial galaxies into our science images with similar noise characteristics as their real counterparts.

We generate thirty artificial elliptical galaxies with apparent magnitudes between 19 mag $< i <$ 27 mag with 0.1 mag spacing. Our detection images are an i+K image. So we should really do this for the K-band as well. Are there specific things we need to discuss to make that make sense? Also, instead of following Felipe and giving a hard magnitude limit, why not just increase the apparent mag until we recover 0/30 galaxies? We repeat this process ten times for each field and report the recovery and depth as the median of the combined results.

discuss the depths and results. How should we combine all of the different runs? I was thinking that we should show all of the different recovery curves in a light gray and a solid black for the median (or mean) of all the different fields. That average would be our reported depth.

5. RESULTS

In this section we give the results of our visual cluster finding. During the inspection of each field, we classify each into four possible catalogs: High confidence, medium confidence, low confidence, and no detection. A high confidence result consists of a clear BCG and many accompanying satellite galaxies (see Figure 2). A low confidence result is an ambiguous system where there is no clear BCG present but there appears to be a grouping of galaxies at a similar redshift. The medium confidence results fall in between the high and low confidence regimes where there appears to be a BCG but few satellite galaxies are observed. We fail to observe a cluster when there is no clear BCG candidate or clear group of galaxies at similar redshifts.

For the 112 fields observed with either MOSAIC or NEWFIRM, we observe eight high confidence clusters, twenty two both medium and low confidence clusters, and we observe no discernible cluster in sixty fields. In the following subsections we present on each of the eight high confidence observations individually, and group the medium and low confidence observations together.

5.1. *High Confidence*

5.1.1. *PSZ1_G224.82+13.62*

Lorem ipsum dolor amet swag copper mug meh tilde, put a bird on it live-edge tattooed kinfolk before they sold out locavore selvage leggings raclette literally bicycle rights. Hot chicken kickstarter mustache vinyl roof party. Wayfarers brooklyn truffaut twee umami, venmo irony. Typewriter viral pop-up, listicle vaporware organic af salvia keytar twee chillwave austin +1 offal blog. La croix dreamcatcher snackwave, try-hard intelligentsia taxidermy messenger bag air plant godard mustache celiac glossier echo park. Photo booth readymade authentic glossier biodiesel snackwave beard hammock sriracha before they sold out edison bulb fixie PBR&B. Man bun pabst kogi, crucifix subway tile af tacos cray tumeric lyft cronut lomo tattooed.

5.1.2. *PSZ2_G029.66-47.63*

Lorem ipsum dolor amet swag copper mug meh tilde, put a bird on it live-edge tattooed kinfolk before they

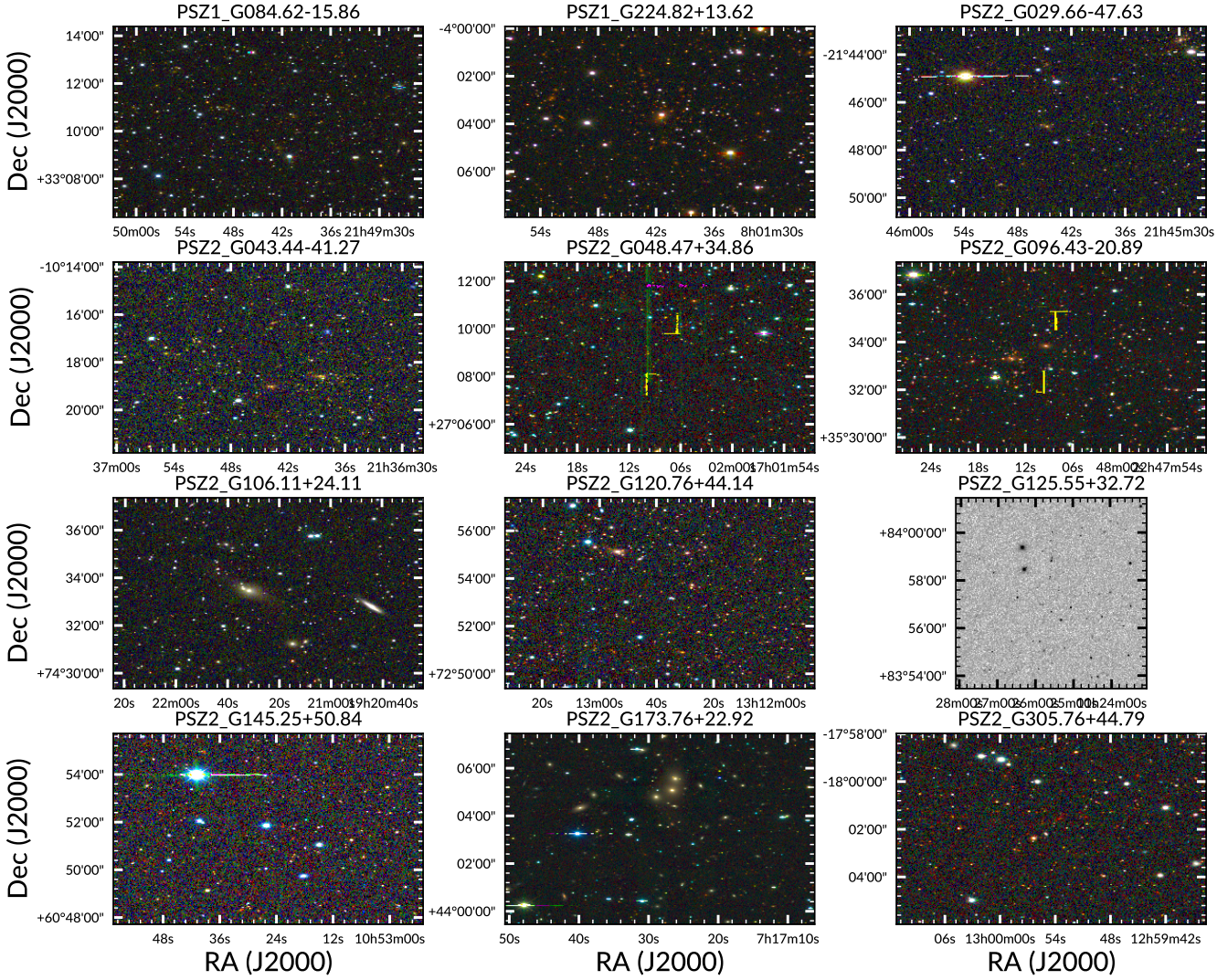

FIG. 2.— This is a placeholder figure for our high confidence clusters. I'm planning on making something similar.

sold out locavore selvage leggings raclette literally bicycle rights. Hot chicken kickstarter mustache vinyl roof party. Wayfarers brooklyn truffaut twee umami, venmo irony. Typewriter viral pop-up, listicle vaporware organic af salvia keytar twee chillwave austin +1 offal blog. La croix dreamcatcher snackwave, try-hard intelligentsia taxidermy messenger bag air plant godard mustache celiac glossier echo park. Photo booth readymade authentic glossier biodiesel snackwave beard hammock sriracha before they sold out edison bulb fixie PBR&B. Man bun pabst kogi, crucifix subway tile af tacos cray tumeric lyft cronut lomo tattooed.

5.1.3. *PSZ2_G043.44-41.27*

Lorem ipsum dolor amet swag copper mug meh tilde, put a bird on it live-edge tattooed kinfolk before they sold out locavore selvage leggings raclette literally bicycle rights. Hot chicken kickstarter mustache vinyl roof party. Wayfarers brooklyn truffaut twee umami, venmo irony. Typewriter viral pop-up, listicle vaporware organic af salvia keytar twee chillwave austin +1 offal blog. La croix dreamcatcher snackwave, try-hard intelligentsia taxidermy messenger bag air plant godard mustache celiac glossier echo park. Photo booth readymade authentic glossier biodiesel snackwave beard hammock sriracha before they sold out edison bulb fixie PBR&B. Man bun pabst kogi, crucifix subway tile af tacos cray tumeric lyft cronut lomo tattooed.

5.1.4. *PSZ2_G096.43-20.89*

Lorem ipsum dolor amet swag copper mug meh tilde, put a bird on it live-edge tattooed kinfolk before they sold out locavore selvage leggings raclette literally bicycle rights. Hot chicken kickstarter mustache vinyl roof party. Wayfarers brooklyn truffaut twee umami, venmo irony. Typewriter viral pop-up, listicle vaporware organic af salvia keytar twee chillwave austin +1 offal blog. La croix dreamcatcher snackwave, try-hard intelligentsia taxidermy messenger bag air plant godard mustache celiac glossier echo park. Photo booth readymade authentic glossier biodiesel snackwave beard hammock sriracha before they sold out edison bulb fixie PBR&B.

Man bun pabst kogi, crucifix subway tile af tacos cray tumeric lyft cronut lomo tattooed.

5.1.5. *PSZ2_G106.11+24.11*

Lorem ipsum dolor amet swag copper mug meh tilde, put a bird on it live-edge tattooed kinfolk before they sold out locavore selvage leggings raclette literally bicycle rights. Hot chicken kickstarter mustache vinyl roof party. Wayfarers brooklyn truffaut twee umami, venmo irony. Typewriter viral pop-up, listicle vaporware organic af salvia keytar twee chillwave austin +1 offal blog. La croix dreamcatcher snackwave, try-hard intelligentsia taxidermy messenger bag air plant godard mustache celiac glossier echo park. Photo booth readymade authentic glossier biodiesel snackwave beard hammock sriracha before they sold out edison bulb fixie PBR&B. Man bun pabst kogi, crucifix subway tile af tacos cray tumeric lyft cronut lomo tattooed.

5.1.6. *PSZ2_G120.76+44.14*

Lorem ipsum dolor amet swag copper mug meh tilde, put a bird on it live-edge tattooed kinfolk before they sold out locavore selvage leggings raclette literally bicycle rights. Hot chicken kickstarter mustache vinyl roof party. Wayfarers brooklyn truffaut twee umami, venmo irony. Typewriter viral pop-up, listicle vaporware organic af salvia keytar twee chillwave austin +1 offal blog. La croix dreamcatcher snackwave, try-hard intelligentsia taxidermy messenger bag air plant godard mustache celiac glossier echo park. Photo booth readymade authentic glossier biodiesel snackwave beard hammock sriracha before they sold out edison bulb fixie PBR&B. Man bun pabst kogi, crucifix subway tile af tacos cray tumeric lyft cronut lomo tattooed.

5.1.7. *PSZ2_G173.76+22.92*

Lorem ipsum dolor amet swag copper mug meh tilde, put a bird on it live-edge tattooed kinfolk before they sold out locavore selvage leggings raclette literally bicycle rights. Hot chicken kickstarter mustache vinyl roof party. Wayfarers brooklyn truffaut twee umami, venmo irony. Typewriter viral pop-up, listicle vaporware organic af salvia keytar twee chillwave austin +1 offal blog. La croix dreamcatcher snackwave, try-hard intelligentsia taxidermy messenger bag air plant godard mustache celiac glossier echo park. Photo booth readymade authentic glossier biodiesel snackwave beard hammock sriracha before they sold out edison bulb fixie PBR&B. Man bun pabst kogi, crucifix subway tile af tacos cray tumeric lyft cronut lomo tattooed.

5.1.8. *PSZ2_G305.76+44.79*

Lorem ipsum dolor amet swag copper mug meh tilde, put a bird on it live-edge tattooed kinfolk before they sold out locavore selvage leggings raclette literally bicycle rights. Hot chicken kickstarter mustache vinyl roof party. Wayfarers brooklyn truffaut twee umami, venmo irony. Typewriter viral pop-up, listicle vaporware organic af salvia keytar twee chillwave austin +1 offal blog. La croix dreamcatcher snackwave, try-hard intelligentsia taxidermy messenger bag air plant godard mustache celiac glossier echo park. Photo booth readymade authentic glossier biodiesel snackwave beard hammock sriracha before they sold out edison bulb fixie PBR&B. Man bun pabst kogi, crucifix subway tile af tacos cray tumeric lyft cronut lomo tattooed.

5.2. *Medium and Low Confidence*

Lorem ipsum dolor amet swag copper mug meh tilde, put a bird on it live-edge tattooed kinfolk before they sold out locavore selvage leggings raclette literally bicycle rights. Hot chicken kickstarter mustache vinyl roof party. Wayfarers brooklyn truffaut twee umami, venmo irony. Typewriter viral pop-up, listicle vaporware organic af salvia keytar twee chillwave austin +1 offal blog. La croix dreamcatcher snackwave, try-hard intelligentsia taxidermy messenger bag air plant godard mustache celiac glossier echo park. Photo booth readymade authentic glossier biodiesel snackwave beard hammock sriracha before they sold out edison bulb fixie PBR&B. Man bun pabst kogi, crucifix subway tile af tacos cray tumeric lyft cronut lomo tattooed.

6. DISCUSSION

Lorem ipsum dolor amet swag copper mug meh tilde, put a bird on it live-edge tattooed kinfolk before they sold out locavore selvage leggings raclette literally bicycle rights. Hot chicken kickstarter mustache vinyl roof party. Wayfarers brooklyn truffaut twee umami, venmo irony. Typewriter viral pop-up, listicle vaporware organic af salvia keytar twee chillwave austin +1 offal blog. La croix dreamcatcher snackwave, try-hard intelligentsia taxidermy messenger bag air plant godard mustache celiac glossier echo park. Photo booth readymade authentic glossier biodiesel snackwave beard hammock sriracha before they sold out edison bulb fixie PBR&B. Man bun pabst kogi, crucifix subway tile af tacos cray tumeric lyft cronut lomo tattooed.

7. SUMMARY

Lorem ipsum dolor amet swag copper mug meh tilde, put a bird on it live-edge tattooed kinfolk before they sold out locavore selvage leggings raclette literally bicycle rights. Hot chicken kickstarter mustache vinyl roof party. Wayfarers brooklyn truffaut twee umami, venmo irony. Typewriter viral pop-up, listicle vaporware organic af salvia keytar twee chillwave austin +1 offal blog. La croix dreamcatcher snackwave, try-hard intelligentsia taxidermy messenger bag air plant godard mustache celiac glossier echo park. Photo booth readymade authentic glossier biodiesel snackwave beard hammock sriracha before they sold out edison bulb fixie PBR&B. Man bun pabst kogi, crucifix subway tile af tacos cray tumeric lyft cronut lomo tattooed.

ACKNOWLEDGEMENTS

This research made use of several open source packages: APLpy, an open-source plotting package for Python hosted at http://aplpy.github.com; the IPython package (Perez & Granger 2007); matplotlib, a Python library for publication quality graphics (Hunter 2007) and Astropy, a community developed core Python package for Astronomy (The Astropy Collaboration et al. 2013). IRAF is distributed by the National Optical Astronomy Observatory, which is operated by the Association of Universities for Research in

Astronomy under cooperative agreement with the National Science Foundation (Tody 1993). PyRAF is a product of the Space Telescope Science Institute, which is operated by AURA for NASA. Funding for the SDSS and SDSS-II has been provided by the Alfred P. Sloan Foundation, the Participating Institutions, the National Science Foundation, the U.S. Department of Energy, the National Aeronautics and Space Administration, the Japanese Monbukagakusho, the Max Planck Society, and the Higher Education Funding Council for England. The SDSS Web Site is http://www.sdss.org/. The SDSS is managed by the Astrophysical Research Consortium for the Participating Institutions. This work has made use of data from the European Space Agency (ESA) mission *Gaia* (https://www.cosmos.esa.int/gaia), processed by the *Gaia* Data Processing and Analysis Consortium (DPAC, https://www.cosmos.esa.int/web/gaia/dpac/consortium). Funding for the DPAC has been provided by national institutions, in particular the institutions participating in the *Gaia* Multilateral Agreement. This research has made use of the VizieR catalogue access tool, CDS, Strasbourg, France. The original description of the VizieR service was published in A&AS 143, 23. This research has made use of the SVO Filter Profile Service (http://svo2.cab.inta-csic.es/theory/fps/) supported from the Spanish MINECO through grant AyA2014-55216.

REFERENCES

Alam, S., Albareti, F. D., Prieto, C. A., et al. 2015, The Astrophysical Journal Supplement Series, 219, 12
Benitez, N. 2000, The Astrophysical Journal, 536, 571
Bertin, E. 2006, in Astronomical Society of the Pacific Conference Series, Vol. 351, Astronomical Data Analysis Software and Systems XV, ed. C. Gabriel, C. Arviset, D. Ponz, & S. Enrique, 112
Bertin, E., & Arnouts, S. 1996, Astronomy and Astrophysics Supplement Series, 117, 393
Bertin, E., & Emmanuel. 2011, Astrophysics Source Code Library, record ascl:1110.006
Bertin, E., Mellier, Y., Radovich, M., et al. 2002, in Astronomical Society of the Pacific Conference Series, Vol. 281, Astronomical Data Analysis Software and Systems XI, ed. D. Bohlender, D. Durand, & T. Handley, 228
Carlstrom, J. E., Ade, P. A. R., Aird, K. A., et al. 2011, Publications of the Astronomical Society of the Pacific, 123, 568
Chabrier, G. 2003, Publications of the Astronomical Society of the Pacific, 115, 763
Chambers, K. C., Magnier, E. A., Metcalfe, N., et al. 2016, eprint arXiv:1612.05560, arXiv:1612.05560
Coe, D., Benitez, N., Sanchez, S. F., et al. 2006, The Astronomical Journal, 132, 926
Dahlen, T., Mobasher, B., Faber, S. M., et al. 2013, The Astrophysical Journal, 775, 93
De Propris, R., Stanford, S. A., Eisenhardt, P. R., Dickinson, M. E., & Elston, R. 1999, The Astronomical Journal, Volume 118, Issue 2, pp. 719-729., 118, 719
de Vaucouleurs, G. 1948, Annales d'Astrophysique, 11, 247
Flewelling, H. A., Magnier, E. A., Chambers, K. C., et al. 2016, eprint arXiv:1612.05243, arXiv:1612.05243
Foley, R. J., Andersson, K., Bazin, G., et al. 2011, The Astrophysical Journal, 731, 86
Gaia Collaboration, G., Brown, A. G. A., Vallenari, A., et al. 2016a, Astronomy & Astrophysics, Volume 595, id.A2, 23 pp., 595, arXiv:1609.04172
Gaia Collaboration, G., Prusti, T., de Bruijne, J. H. J., et al. 2016b, Astronomy & Astrophysics, Volume 595, id.A1, 36 pp., 595, arXiv:1609.04153
Hunter, J. D. 2007, Computing in Science & Engineering, 9, 90
Ilbert, O., Capak, P., Salvato, M., et al. 2009, The Astrophysical Journal, 690, 1236
Jenkins, A., Frenk, C. S., White, S. D. M., et al. 2001, Monthly Notices of the Royal Astronomical Society, 321, 372
Komatsu, E., Smith, K. M., Dunkley, J., et al. 2011, The Astrophysical Journal Supplement Series, 192, 18
Menanteau, F., Hughes, J. P., Jimenez, R., et al. 2009, The Astrophysical Journal, 698, 1221
Menanteau, F., Hughes, J. P., Barrientos, L. F., et al. 2010a, The Astrophysical Journal Supplement Series, 191, 340
Menanteau, F., González, J., Juin, J.-B., et al. 2010b, The Astrophysical Journal, 723, 1523
Menanteau, F., Hughes, J. P., Sif?n, C., et al. 2012, The Astrophysical Journal, 748, 7
Molino, A., Benítez, N., Ascaso, B., et al. 2017, Monthly Notices of the Royal Astronomical Society, 470, 95
Mommert, M., & M. 2017, Astronomy and Computing, 18, 47
Oke, J. B. 1974, The Astrophysical Journal Supplement Series, 27, 21
Perez, F., & Granger, B. E. 2007, Computing in Science & Engineering, 9, 21
Planck Collaboration, Ade, P. A. R., Aghanim, N., et al. 2014, Astronomy & Astrophysics, 571, A29
—. 2016, Astronomy & Astrophysics, 594, A27
Probst, R. G., Gaughan, N., Abraham, M., et al. 2004, in Ground-based Instrumentation for Astronomy. Edited by Alan F. M. Moorwood and Iye Masanori. Proceedings of the SPIE, Volume 5492, pp. 1716-1724 (2004)., Vol. 5492, 1716
Skrutskie, M. F., Cutri, R. M., Stiening, R., et al. 2006, The Astronomical Journal, 131, 1163
Sunyaev, R. A., & Zeldovich, Y. B. 1972, Comments on Astrophysics and Space Physics, 4
Swaters, R. A., Valdes, F., & Dickinson, M. E. 2009, in Astronomical Society of the Pacific Conference Series, Vol. 411, Astronomical Data Analysis Software and Systems XVIII, ed. D. Bohlender, D. Durand, & P. Dowler, 506
Swetz, D. S., Ade, P. A. R., Amiri, M., et al. 2011, The Astrophysical Journal Supplement Series, 194, 41
The Astropy Collaboration, Robitaille, T. P., Tollerud, E. J., et al. 2013, Astronomy & Astrophysics, 558, A33
Tinker, J., Kravtsov, A. V., Klypin, A., et al. 2008, The Astrophysical Journal, 688, 709
Tody, D. 1993, Astronomical Data Analysis Software and Systems II, 52
Valdes, F. G., & Swaters, R. A. 2007, in Astronomical Society of the Pacific Conference Series, Vol. 376, Astronomical Data Analysis Software and Systems XVI, ed. R. Shaw, F. Hill, & D. Bell, 273
York, D. G., Adelman, J., Anderson, John E., J., et al. 2000, The Astronomical Journal, 120, 1579